A Diffusion Cloud-Chamber Study of Pion Interactions in Hydrogen and Helium*

E. C. FOWLER,† W. B. FOWLER, R. P. SHUTT, A. M. THORNDIKE, AND W. L. WHITTEMORE
Brookhaven National Laboratory, Upton, New York

(Received March 27, 1953)

A description is given of the operation of a high pressure diffusion cloud chamber filled with hydrogen or helium and exposed to pion beams of both signs and energies near 60 and 100 Mev. Interactions occurring in the gas filling are investigated. The cross sections found in hydrogen agree with the results of others, including the large difference between the cross sections for positive and negative mesons. In helium the total cross sections are 89 ± 18 and 207 ± 27 mb with beams at 60 and 105 Mev, respectively. These cross sections include elastic and inelastic scattering, charge exchange, and absorption. The charge exchange cross sections, estimated at 20 and 60 mb for the two respective energies, are much larger than observed by others for different nuclei. Assuming that the mesons interact with the individual nucleons in the nucleus, an approximate calculation shows that a fairly consistent picture can be obtained making use of phase shifts determined by Anderson *et al.* for meson scattering on hydrogen.

I. INTRODUCTION

INTERACTIONS of pions in hydrogen and helium gas have been observed in a diffusion cloud chamber operated in various pion beams at the Nevis cyclotron[1] of Columbia University. Both results and experimental techniques are discussed in the present article. Since pions are considered to be nuclear-force mesons, an investigation of their interactions with light nuclei is of particular interest. Detailed theoretical predictions concerning the scattering of pions by nucleons on the basis of weak coupling theory have been presented by Ashkin, Simon, and Marshak,[2] and by Peshkin.[3] The strong coupling theory has been applied by Brueckner, leading to quite different results.[4]

At the time this work was started no data were available on the scattering of pions by hydrogen or helium, although a number of cosmic-ray experiments had indicated that pions have an approximately geometrical cross section for interactions with nuclei.[5–8] While this work was in progress a number of pion-proton cross sections were measured by Sachs, Steinberger, and co-workers[9,10] and energy and angular dependences determined by Anderson *et al.*,[11–14] both employing scintillation counter telescopes. Furthermore, data were obtained by Goldhaber and Lederman[15] using nuclear emulsions. Our data are in general agreement with those results and provide an independent confirmation of their correctness. The comparison is made in Sec. V. We are not aware of any other data on helium. Preliminary reports on some of our results have already been given.[16–18]

II. APPARATUS

A. The Diffusion Cloud Chamber

The development of high-pressure diffusion cloud chambers at Brookhaven arose from the need for a cloud chamber for use with the Brookhaven Cosmotron, which could accept pulses once every five seconds (the repetition rate of the machine). Normal pressure expansion cloud chambers of the required size can accept a beam pulse only about once a minute. If it is desired to study events directly in the gas, operation at high pressure becomes necessary, lengthening the cycling time even more. Continuously sensitive cloud chambers were built first by Langsdorf[19] and later by Cowan[20] and by Needels and Nielsen.[21] With the heavier gases diffusion cloud chambers cannot be operated far above normal pressure. However, with the light gases, of particular interest to us, diffusion cloud chambers operate best at pressures from 10 to 50 atmospheres.[22]

We used a diffusion chamber filled with hydrogen or helium at pressures near 20 atmospheres.[16] Its construc-

* Work performed under the auspices of the U. S. Atomic Energy Commission.

† Now at Yale University, New Haven, Connecticut.

[1] Supported jointly by the U. S. Office of Naval Research and the U. S. Atomic Energy Commission.

[2] Ashkin, Simon, and Marshak, Progr. Theoret. Phys. **5**, 634 (1950).

[3] M. Peshkin, Phys. Rev. **81**, 425 (1951).

[4] K. A. Brueckner, Phys. Rev. **86**, 106 (1952).

[5] Camerini, Fowler, Lock, and Muirhead, Phil. Mag. **41**, 413 (1950).

[6] Butler, Rosser, and Barker, Proc. Phys. Soc. (London) **A63**, 145 (1950).

[7] W. W. Brown and A. S. McKay, Phys. Rev. **77**, 342 (1950).

[8] B. P. Gregory and J. H. Tinlot, Phys. Rev. **81**, 667, 675 (1951).

[9] Chedester, Isaacs, Sachs, and Steinberger, Phys. Rev. **82**, 958 (1951).

[10] Isaacs, Sachs, and Steinberger, Phys. Rev. **85**, 803 (1952).

[11] Anderson, Fermi, Long, Martin, and Nagle, Phys. Rev. **85**, 934 (1952).

[12] Anderson, Fermi, Long, and Nagle, Phys. Rev. **85**, 936 (1952).

[13] Anderson, Fermi, Nagle, and Yodh, Phys. Rev. **86**, 793 (1952).

[14] Anderson, Fermi, Martin, and Nagle, Phys. Rev. **91**, 155 (1953).

[15] G. Goldhaber, Phys. Rev. **87**, 220 (1952); G. Goldhaber and L. Lederman, Phys. Rev. **90**, 343 (A) (1953).

[16] Shutt, Fowler, Miller, Thorndike, and Fowler, Phys. Rev. **84**, 1247 (1951).

[17] Thorndike, Fowler, Fowler, and Shutt, Phys. Rev. **85**, 929 (1952).

[18] Fowler, Fowler, Shutt, Thorndike, and Whittemore, Phys. Rev. **86**, 1053 (1952).

[19] A. Langsdorf, Rev. Sci. Instr. **10**, 91 (1939).

[20] E. W. Cowan, Rev. Sci. Instr. **21**, 991 (1950).

[21] T. S. Needels and C. E. Nielsen, Rev. Sci. Instr. **21**, 976 (1950).

[22] Miller, Fowler, and Shutt, Rev. Sci. Instr. **22**, 280 (1951); J. M. Wyckoff, Phys. Rev. **87**, 185 (1952).

tion is indicated by Fig. 1. The chamber consists of welded steel top and bottom cans separated by a bakelite insulating ring.

The bottom can has a $\frac{1}{4}$-in. stainless steel cylinder wall (1), and a 1.25-in. bottom plate (2), and top flange (3), both made from cold rolled steel. There are two rectangular-shaped ducts at opposite sides of the cylinder to provide for windows. Each duct ends in a window face plate (4) provided with an *O*-ring groove. The bottom plate carries a drain for liquid at the center.

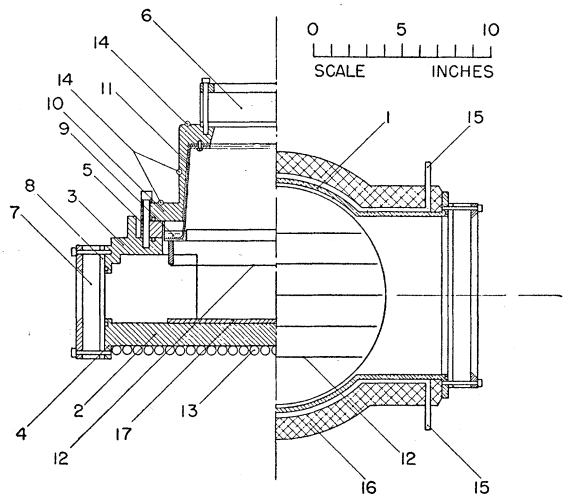

FIG. 1. Diagram of diffusion cloud chamber designed for operation at 20 atmospheres.

The bakelite ring (5), placed between top and bottom cans, is sealed by *O*-rings. The bolts fastening the top to the bottom are thermally insulated from the top by Bakelite washers and fiber sleeves.

The top was made in a hat shape so that the top window (6) could be close to the camera and hence be small in size. In addition, the extra space provides an improved vapor supply.

In principle the construction of each of the three windows is the same. Supported by a 1-in. thick plexiglass slab (7), a $\frac{1}{4}$-in. thick piece of Allite[23] (8) in contact with an *O*-ring seals against the pressure. Special low temperature *O*-rings[24] are used at the side windows. Allite is used because it is not attacked by alcohol. Plastic windows were thought to be superior to glass windows because of the large temperature gradients present in the side windows while under high mechanical stress. Lucite also has a lower thermal conductivity than glass, making it easier to maintain the proper temperature gradients.

The top carries a liquid reservoir in the form of a copper trough (9) in good thermal contact with the top's base plate (10). In order to enhance evaporation from the trough a piece of felt lines the vertical portion of the top (11), and hangs in the trough so that the felt is kept wet by capillary action. A set of five wires (12), 0.025 in. in diameter, spaced $1\frac{7}{8}$ in. apart, is mounted on insulated posts to provide a grid to which an electric sweeping voltage may be applied. The top is pierced by a Kovar-glass lead-through for the sweeping voltage and also by a filling line which terminates just above the copper reservoir trough.

In order to provide temperature control the chamber has cooling coils (13) at the bottom and nichrome heating wires at the top (14) and at the side (15). Furthermore, the chamber is insulated (16) from the surrounding air. These facilities, aided by the bakelite ring, make it reasonably easy to vary the temperature gradient in the side wall while holding the top and bottom temperatures approximately constant.

A circular piece of black glass (17) forms the photographic background. The side walls of the chamber are lined with black velvet, and the inner metallic surfaces of the top are painted with black glyptal where necessary.

B. Auxiliary Equipment

The chamber is cooled by trichloroethylene circulated directly over pieces of dry ice contained in a can. A turbine pump[25] driven by a $\frac{1}{3}$-hp motor pumps 6 gal/min through a screened intake and through the cooling coils of the chamber at a gauge pressure of about 20 lb/in.^{2}. This brings the temperature of the chamber's bottom plate to about -70°C.

The chamber is illuminated by two flash tubes of 4-mm i.d. Vykor tubing, 8 in. long, with tungsten anode and sintered tungsten-bariumoxide cathode,[26] filled with Kr and Xe at pressures of about 20 and 160 mm Hg, respectively. For photographing tracks a 70-μf capacitor at 2000 v is discharged through each tube. The light is focused to a beam about $2\frac{1}{2}$ in. high by parabolic reflectors 8 in. long with focal length $\frac{7}{8}$ in. The reflectors consist of chrome-on-brass ferrotype plates forced into a set of ribs machined to the required parabolic shape. Each parabola is mounted in a sheet metal box through which air is blown to cool the flash tube and reduce condensation on the Lucite windows.[27] Under these conditions flash tubes have a useful life of many thousand flashes. For visual observation of the chamber a 1.0-μf condenser charged to 2000 v is discharged through the flash tube at a rate of about 40 times per second.

Stereoscopic photographs are taken through two *f*/2.3, 30-mm Baltar wide-angle lenses, mounted just above the top window of the chamber. Apertures of

[23] Procured from the Homalite Corporation, Wilmington, Delaware, and Cast Optics Corporation, Riverside, Connecticut.

[24] Procured from Linear Incorporated, Philadelphia, Pennsylvania.

[25] Procured from Aurora Pump Company, New York, New York.

[26] Procured from P. R. Mallory Company, Indianapolis, Indiana.

[27] Fogging of the windows at the outside is prevented by occasional wiping with "Photo-Flo," procured from Eastman Kodak Company, Rochester, New York.

$f/5.6$ or $f/8$ are normally used. Each lens views the center of the chamber at an angle of about 8°. Interchangeable film magazines fit into the lens mount, holding 100 ft of 35-mm film, normally unperforated Linagraph Ortho. Film is advanced by a motor drive so that the two stereo views are interspaced on the same film.

Timing circuits are necessary to determine the overall repetition rate and the timing of sweeping field, cyclotron beam, light flash, and camera film advance. The sequence of operations is indicated in Fig. 2, and typical time intervals are given. All the necessary timing is achieved by means of delay units consisting of *RC* circuits on the grids of 2D21 tubes driving Struthers-Dunn relays. Each unit controls an operation and starts the next unit. The last one removes the plate voltage, which resets all units. The delays are variable over wide ranges and have proved to be reliable and sufficiently accurate for the purpose.

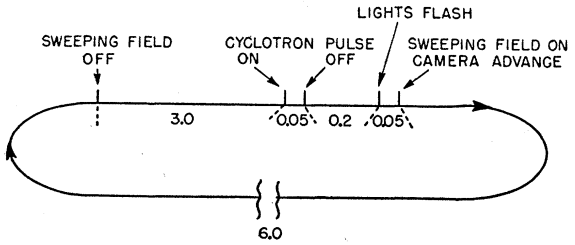

FIG. 2. Schematic cycle of operations with typical time delays indicated. All times are in seconds.

III. OPERATION OF DIFFUSION CHAMBER

A. General Procedure

Light gases can be employed conveniently in diffusion cloud chambers if the pressure is increased appropriately.[22,28] In these experiments either hydrogen at about 300 lb/in.^{2} pressure (above atmospheric) or helium at about 200 lb/in.^{2} were employed. The vapor used has been methyl alcohol in all cases. It has desirable properties of high vapor pressure, low freezing point, and low critical supersaturation for the formation of droplets.

The temperature of the bottom of the chamber is kept at about −70°C. The top of the chamber is kept at about 15°C. Since it is insulated from the bottom by the bakelite ring, its temperature is fairly uniform. Practically all the gradient occurs across the bakelite ring and along the side wall of the bottom part of the chamber. Just below the bakelite ring the temperature is kept at about 0°C. This leaves a gradient of about 7°C per cm in the side wall of the chamber. Under these conditions a sensitive layer 6-7 cm deep may be obtained at the bottom of the chamber. Conditions in the chamber vary considerably, and the largest droplets are found near the top of the sensitive layer. Nevertheless photographs of tracks passing through the sensitive layer rarely show a marked change in density except near the top or bottom.

The depth of the sensitive layer can be increased by making the bottom colder. By reducing the temperature to −90°C an increase of about 2 cm in layer depth was obtained, but the tracks near the bottom were rather thin and slow-forming because of the very low vapor pressure at the bottom. This procedure was not employed during runs with the cyclotron. If the top temperature is raised to increase the vapor supply, a background fog with a cellular structure appears with H_2 or He fillings. This is believed to be caused by local turbulent currents induced by the heat released by the condensation process. If the temperature gradient is reduced, tracks become less dense and the sensitive layer may lift off the bottom of the chamber. The temperature distribution described gave the deepest layer of satisfactory quality. These observations are in agreement with theoretical estimates.[28]

Since the supply of vapor existing in the gas is limited, it may be exhausted by excessive ionization in the chamber, in which case the chamber becomes completely insensitive. A continuous intensity need only be 3 to 10 times (depending on the gas and pressure used) cosmic-ray intensity to do this. If the source of radiation is removed, the chamber recovers in about one minute. In experiments with the cyclotron-produced meson beam a short pulse of fairly high intensity passes through the chamber, which then has a recovery period before the next pulse. Under such conditions intensities many times cosmic-ray intensity are possible as long as the average intensity does not become too great. Under some conditions the chamber may be locally insensitive. A dense background track may take enough vapor from a certain region to make it temporarily insensitive. A beam track passing through this region shortly afterward will then have a "gap" in it due to this insensitivity. Such gaps have, in fact, been frequent, and have made the analysis of the pictures obtained more difficult. These effects are caused both by background particles passing through the sensitive layer of the chamber and by those passing above it. The ions formed above the sensitive layer diffuse down into it and then act as nuclei for the formation of droplets, either in the form of a uniform "rain" or as broad diffuse tracks.

The chamber can be made more radiation-resistant by the application of an electric sweeping field, especially in the case where the radiation occurs mainly in pulses. The sweeping field is turned on for a period after the pulse and serves mainly to sweep out ions formed in the upper part of the chamber before they can diffuse into the sensitive region. The sweeping field does, however, sweep some ions into the sensitive region and causes some distortion of tracks formed in the sensitive region, so that it should be turned off some time before the desired particles pass through the

[28] R. P. Shutt, Rev. Sci. Instr. **22**, 730 (1951).

chamber, as shown in Fig. 2. In most cases the sweeping field potential has been about 1000 v.

B. Operation with the Nevis Cyclotron

The experiments reported here were all carried out using pion beams produced at the Columbia University Nevis cyclotron. The pions were produced in an internal target, partially focussed in the fringing field of the cyclotron, and allowed to emerge through holes in the six-foot thick concrete shield of the cyclotron. The arrangement is shown in Fig. 3. The cyclotron beam was controlled by pulsing the ion source, usually with a cycle time of about six or eight seconds. The number of particles traversing the chamber could be adjusted by changing the pulse length. The cyclotron usually ran with a repetition rate of 40 to 80 per sec and the beam pulse was long enough to include one to four cycles, or occasionally more.

In most cases the diffusion chamber was run concurrently with the Columbia 16-in. expansion chamber.[29] During the recovery period of the expansion chamber the diffusion chamber was automatically cut in, operated for six to eight beam pulses, then cut out when the expansion chamber was ready for a pulse. This procedure was quite successful on the whole, although there was some difficulty in obtaining meson-beam intensities satisfactory for both chambers.

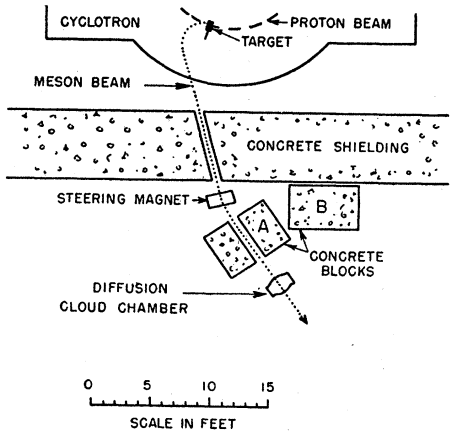

FIG. 3. Position of cloud chamber, steering magnet, and shielding, relative to cyclotron.

The steering magnet deflected the pions out of the direct line of sight through the hole in the shielding. Concrete shielding blocks were necessary to reduce background. In lining up the equipment and during operation a beam monitor consisting of two scintillation counters in coincidence proved very useful. Despite all these precautions high background remained one of the chief problems, consisting of both particles occurring between desired beam pulses and particles occurring at the time of the beam pulse but with random directions.

[29] Byfield, Kessler, and Lederman, Phys. Rev. **86**, 17 (1952).

Under these conditions it has been possible to obtain about 10–20 beam tracks per pulse with fairly good picture quality. Pictures were taken at a rate of about 400 per hour, so that a typical two-shift day resulted in about 5000 pictures, allowing some time lost for setting up, adjustment, and repair of minor casualties.

IV. RESULTS

A. Pictures Obtained

Major portions of eight days of cyclotron operation were required to obtain the pictures upon which we are now reporting. In an attempt to survey the various interactions which might be studied with a diffusion chamber, H_2 and He fillings were employed, each with positive and negative pions of about 60 Mev and negative pions of about 100 Mev. The conditions of the various runs are summarized in Table I, where the pion energies inside the chamber are listed. A total of 33 700 pictures were taken and analyzed. On the average each picture has about 10 pion tracks.

TABLE I. Summary of pictures obtained.

Day	Gas	Beam	No. of pictures
6 April 1951	H_2	60-Mev π^-	5600
1 June 1951	He	53-Mev π^+	3400
28–29 June 1951	H_2	53-Mev π^+	8400
28–29 January 1951	He	68-Mev π^-	5700
3 June 1952	H_2	105-Mev π^-	5400
11 June 1952	He	105-Mev π^-	5200

B. Analysis of Pictures

The analysis of the pictures was carried out in two steps; the films were first scanned and interesting events noted, then each event was analyzed in detail. For scanning modified Stereo-Vivid projectors[30] were used, which enabled either stereo view to be thrown upon the screen. By looking at the image obliquely, so that the beam tracks are foreshortened, any deflection is readily recognized. Under these conditions confusion due to background tracks is much reduced. Once the procedure was established, the majority of the scanning was done by nonscientific personnel, as has often been done in nuclear emulsion work.

For analysis of the scattering events a projector was built in which the camera lenses could be used in the same geometry as employed for taking pictures. The two stereo images were made to coincide on a ground glass screen by properly adjusting its position in space.[31] In this way the true lengths of tracks and angles between them were measured.

During the scanning each beam track was inspected, as in "along-the-track" scanning in emulsions,[32] and

[30] Procured from Three Dimension Company, Chicago, Illinois.
[31] W. Powell, Rev. Sci. Instr. **20**, 402 (1949).
[32] Bernardini, Booth, Lederman, and Tinlot, Phys. Rev. **82**, 105 (1951).

any event was noted which might possibly be a pion interaction. In addition all decays in flight of pions (π) into mesons (μ) with projected angles of 4° or more (in either view) were recorded. (Such π-μ decays appear as sudden deflections of straight tracks without the recoil track characteristic of a scattering event.) About 20 percent of the pictures were scanned twice independently as a check on the consistency of the scanning procedure and on scanning efficiency. The number of π-μ decays checked was great enough that the discrepancies could be used to estimate the probability that a single observer would find a π-μ. This scanning efficiency was determined to be 86 percent, 91 percent, 83 percent, 93 percent, 88 percent, and 87 percent on the various runs (in the order appearing in Table I). For pion-interaction events the probability of detection should be somewhat higher, since they are easier to recognize. It seems certain that not many events were missed.

A considerable number of events were noted during scanning which were not pion interactions. When the events were reprojected and analyzed the following criteria were used to determine whether the event was acceptable: (1) Incoming track must be straight and in the direction of the meson beam. (2) Angles between tracks must be consistent with those expected for a pion interaction, in particular, an elastic scattering must be coplanar, with the right angular relationships. (3) Lengths of recoil tracks must be consistent with those expected. (4) Densities of tracks must be reasonably consistent with those expected. These considerations usually determine whether the event is a pion interaction or not, although there are a few doubtful cases. In particular, scatterings with small scattering angle and very short recoil are always doubtful, and elastic scatterings through less than 20° were not counted.

C. Determination of Pion Path Length

The number of π-μ decays observed is used as an indication of the total path length of the pions that have traversed the cloud chamber. The mean path length for decay of a pion of momentum p, rest mass μ_0, and rest lifetime τ_0, is

$$X=p\tau_0/\mu_0. \quad (1)$$

Taking $\tau_0=2.55\times10^{-8}$ sec,[33–35] and $\mu_0=277m_e$,[36] this gives (X in cm, pc in Mev)

$$X=5.44pc. \quad (2)$$

From this length and the average gas density in the sensitive depth the path length in g/cm² per π-μ decay is calculated.

[33] Lederman, Byfield, and Kessler, Phys. Rev. **85**, 719 (1952).
[34] W. L. Kraushaar, Phys. Rev. **86**, 513 (1952).
[35] Durbin, Loar, and Havens, Phys. Rev. **88**, 179 (1952).
[36] Barkas, Smith, and Gardner, Phys. Rev. **82**, 102 (1951).

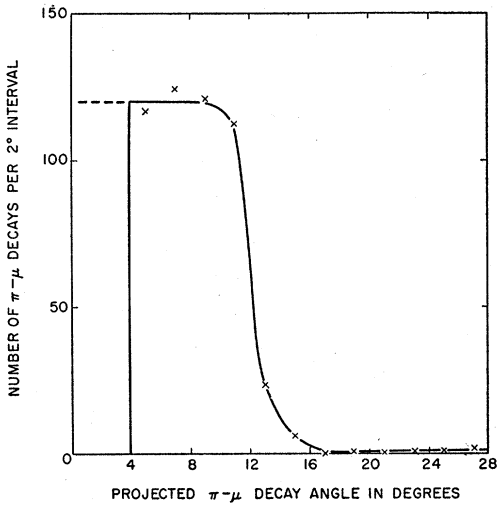

FIG. 4. Typical distribution of projected π-μ angles. The points shown were obtained for the 105-Mev π^- beam which gave the sharpest cutoff.

To obtain the total number of π-μ decays a correction must be made to the number of π-μ's counted to take account of those with projected angles less than 4°. This correction is determined by plotting the distribution of π-μ decay angles, as in Fig. 4. The dotted curve gives the number of π-μ's of small angle that were not counted. (While the distribution of true π-μ angles in space is peaked at the maximum angle, calculation shows that the projected angle distribution should be quite flat for the present pion energies.) The correction factor is therefore the ratio of the total area under the curve to that under the solid part. The cut-off angle of the distribution is also useful since it provides a measure of the pion momentum. A broad distribution of pion momenta would lead to a gradual decline rather than the sharp cut-off seen in Fig. 4.

The π-μ counts and π-path lengths derived from them are given in Table II.

D. Interactions Observed

The numbers of interactions observed are given in Table III. From the numbers of interactions and the π-μ decays the path lengths and cross sections for interactions can be calculated. These results are also given in Table III. Statistical standard errors are

TABLE II. Pion path lengths observed.

Gas	Beam	π-μ count $\theta\geqq4°$ in left view	Correction factor	Path length per π-μ g/cm²	Total path length g/cm²
H_2	60-Mev π^-	642	1.32	1.65	1400
H_2	53-Mev π^+	967	1.24	1.49	1780
H_2	105-Mev π^-	504	1.54	2.22	1720
He	68-Mev π^-	298	1.35	2.16	865
He	53-Mev π^+	345	1.25	2.12	915
He	105-Mev π^-	516	1.47	3.09	2340

TABLE III. Summary of interactions.

Filling	Beam	Number of inter-actions	Interaction path length g/cm²	Cross section in millibarns (10^{-27} cm²)
H_2	60-Mev π^-	3	470	3.5±2
H_2	53-Mev π^+	21	85	22±5
H_2	105-Mev π^-	11	160	11±3
He	68-Mev π^-	11	79	84±26
He	53-Mev π^+	13	70	95±27
He	105-Mev π^-	72	33	207±24

quoted. The cross sections calculated directly from the number of observed interactions have been increased by 5 percent–13 percent to correct for the elastic scatterings through less than 20° which were not counted. The amount of correction depends on the amount of elastic scattering and on the shape of the angular distribution above 20°.

It is not likely that any of the observed interactions listed in Table III involved carbon or oxygen in the alcohol rather than H_2 or He. At our operating pressures there is at most (at the top of the sensitive layer) one molecule of methyl alcohol per 800 molecules of H_2 or 600 atoms of He. In addition interactions of pions with C or O would certainly not be confused with elastic scatterings from H_2 or He and would not be expected to resemble inelastic scatterings or absorptions in the light elements very often. A few pion interactions apparently involving C or O were observed in addition to those given in Table III.

V. DISCUSSION OF HYDROGEN DATA

In the case of hydrogen, negative pions (π^-) can undergo elastic scattering, charge exchange scattering, or radiative capture, while positive pions (π^+) undergo elastic scattering only. The reactions are given in Eq. (3). Only the elastic scatterings were observed in the cloud chamber:

$$\begin{aligned} &\pi^-+p\rightarrow\pi^-+p && \text{(elastic)}\\ &\pi^-+p\rightarrow\pi^0+n && \text{(charge exchange)}\\ &\pi^-+p\rightarrow\gamma+n && \text{(radiative capture)}\\ &\pi^++p\rightarrow\pi^++p && \text{(elastic).} \end{aligned} \tag{3}$$

The other interactions should appear as beam meson tracks disappearing without recoil or scattered particle. Because of the frequent gaps in tracks and insensitive areas in the chamber such disappearances were not generally recognizable, although one definite example was noticed. Consequently, the hydrogen cross section given in Table III for π^+ is the total cross section while those given for π^- are not. Results obtained at Chicago indicate that elastic scattering is only about $\frac{1}{3}$ the total cross section for π^- at 118 Mev.[37] Radiative capture is thought to be small (see Sec. VI).

The cross sections here reported for π^- suggest that also at 60 Mev elastic scattering of π^- is much smaller than the total cross section. The cross section for π^+ is consistent with the Chicago data. A summary of cross sections reported in the literature[9–14,38] is given in Fig. 5.

From the π^+-p scattering events at 53 Mev it was possible to obtain some information concerning the angular distribution. As previously reported[18] the scatterings are concentrated in the forward and backward directions. They are consistent with $\cos^2\theta_0$ or $(1+3\cos^2\theta_0)$ distributions (θ_0 is the angle in the center-of-mass system), but not with an isotropic one, indicating that p-wave scattering is important at these energies. However, because of the large statistical errors, there may also be some s-wave scattering. This would lead to asymmetries in the distributions as observed by the Chicago group at higher energies.[13,14]

VI. DISCUSSION OF HELIUM DATA

A. Experimental Cross Sections

When a pion strikes a helium nucleus, the interactions shown in Eq. (4) can take place. The combination $(2p+2n)$, for instance, signifies

$$\pi^++\mathrm{He}\rightarrow\pi^++\mathrm{He},\quad \pi^-+\mathrm{He}\rightarrow\pi^-+\mathrm{He} \quad \text{(elastic)} \tag{4a}$$

$$\rightarrow\pi^++(2p+2n),\quad \rightarrow\pi^-+(2p+2n) \quad \text{(inelastic)} \tag{4b}$$

$$\rightarrow\pi^0+(3p+n),\quad \rightarrow\pi^0+(p+3n) \quad \text{(charge exchange)} \tag{4c}$$

$$\rightarrow(3p+n)\quad \rightarrow(p+3n) \quad \text{(absorption)}, \tag{4d}$$

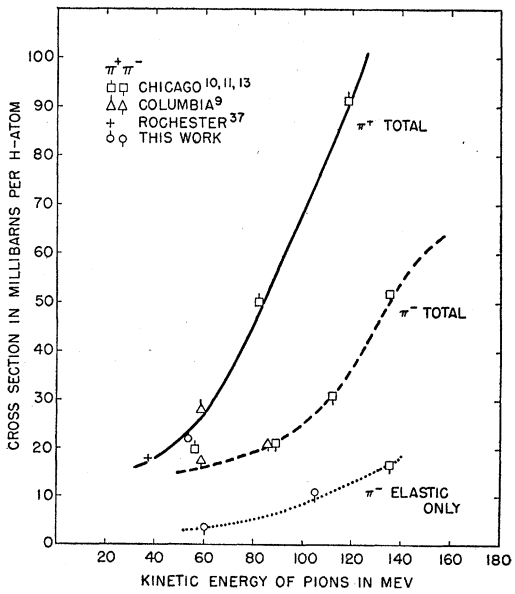

FIG. 5. Summary of cross sections obtained by various experimenters for π-p scattering. The solid curve gives the π^+-p cross section, the dashed curve the total π^--p, and the dotted curve the elastic π^--p cross section only. The highest energy points obtained at Chicago are off scale on this graph.

[37] Fermi, Anderson, Lundby, Nagle, and Yodh, Phys. Rev. **85**, 935 (1952).

[38] Barnes, Clark, Perry, and Angell, Phys. Rev. **87**, 669 (1952).

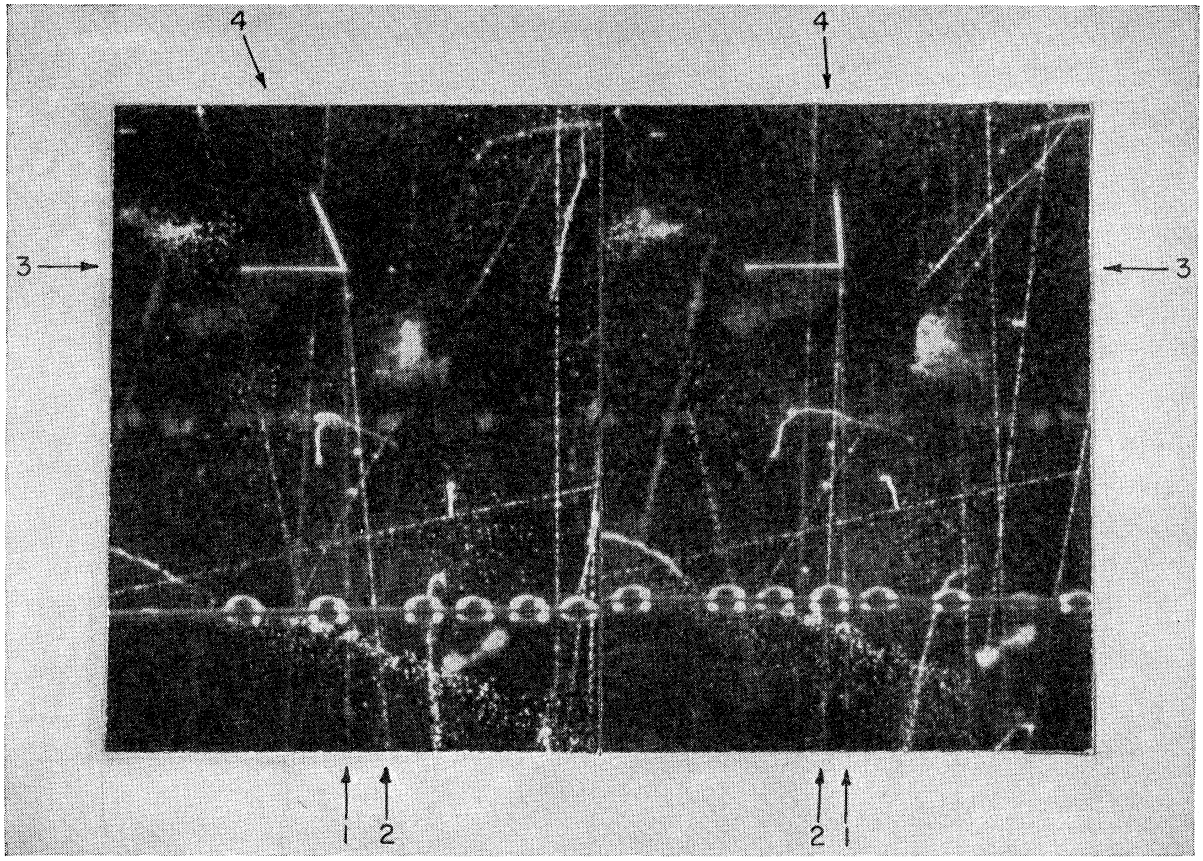

FIG. 6. Photograph of a 105-Mev negative pion scattered inelastically in helium. Tracks 1 and 2 show incident and scattered pions, respectively. Tracks 3 and 4 are two charged recoils, both stopping in the gas.

two protons and two neutrons, some of which may be bound together as He^3, H^3, or H^2.

The pion may be scattered elastically with cross section σ_e [Eq. (4a)], or the interaction may lead to a reaction with cross section σ_r [Eq. (4b, c, d)]. The total cross section is therefore $\sigma_t=\sigma_e+\sigma_r$. Examples of photographs are given in Figs. 6 and 7.

σ_r can be split into several other cross sections. The pion can transfer enough energy to the constituent nucleons of the nucleus to excite the latter. Since helium has no excited states except for a broad level near its binding energy of 28 Mev, this will practically always result in a disintegration of the nucleus [Eq. (4b)]. In addition to the incoming meson track, one therefore should see a track of a considerably slowed-down meson and either one heavily ionized track due to a He^3 nucleus, or two such tracks attributable to H^3+H^1, $2H^2$, or $2H^1$ (Fig. 6). σ_i shall stand for the cross section for these events. The other class of events results in a transfer of the electric charge of the meson to a nucleon [Eqs. (4c) and (4d)], with a cross section σ_c so that $\sigma_r=\sigma_i+\sigma_c$. Here no meson track can be seen after the collision (Fig. 7). If the meson had positive charge, 2 or 3 heavily ionized tracks will emerge, consisting of He^3+H^1, H^2+2H^1, or $3H^1$. If the meson was negative there will be only one heavy track after the collision consisting of H^3, H^2, or H^1.

σ_c can be subdivided further. The transfer of charge may either have occurred by a scattering of the meson with charge exchange, [Eq. (4c)], with cross section σ_γ, or by absorption of the meson [Eq. (4d)], with cross section σ_α. Therefore $\sigma_c=\sigma_\alpha+\sigma_\gamma$. The pion can be absorbed by a single nucleon, resulting in a gamma-ray and a recoil particle, or by several nucleons simultaneously, resulting in several recoil particles of fairly high energy exhibiting a certain amount of correlation between their directions of flight. Without application of a magnetic field for momentum measurements some difficulty is encountered in deciding whether a particular event classified under σ_c belongs to σ_α or σ_γ. For π^+, where three outgoing prongs are visible, a conclusion might be drawn from the spatial correlation of the prongs, their range, and their apparent density of ionization. However, for π^- events, with only one outgoing prong, no such arguments are available.

As stated above, observations were made with π^+ at 53 Mev, and with π^- at 68 and 105 Mev. The observed

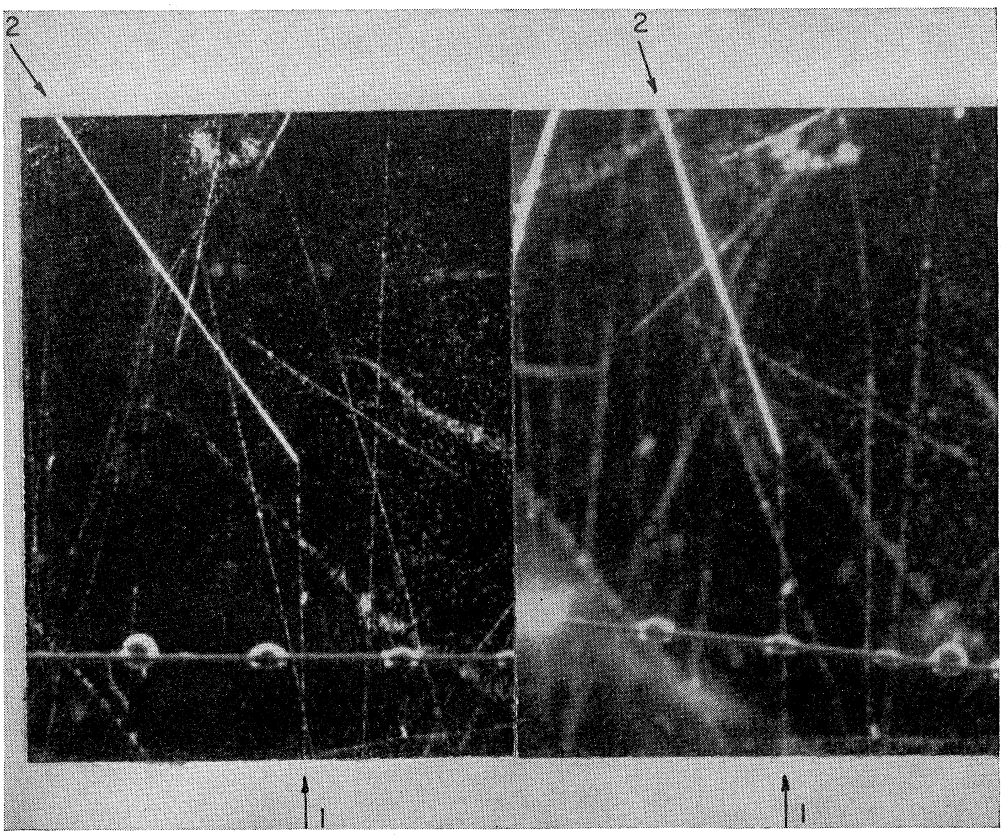

FIG. 7. Photograph of charge exchange or absorption of a 105-Mev negative pion. Track 1 is the incident pion and Track 2 is the only charged recoil.

frequencies of the different types of interactions are compiled in Table IV.

The absorption event noted for π^+ at 53 Mev has been exhibited previously.[17] It shows what are believed to be two fairly fast protons emerging in almost opposite directions, and a third short, heavy track. The four other events noted under "charge transfer" are believed to be caused by charge exchange for the following reasons. Since the maximum energy transfer from a 53-Mev pion to a nucleon is about equal to the total binding energy of 28 Mev of the helium nucleus, one might expect that the most probable event to happen after a charge exchange would be a disintegration of He^4 into He^3+H^1 requiring only 21 Mev. In such a break-up the proton, formed by collision with charge exchange of the incoming π^+ with a neutron, would receive most of the available energy. The He^3 particle, receiving only a small portion of the energy, loses its energy quite fast because of its twofold electric charge and thus exhibits a very short range. Therefore at the present fairly low energy a π^+ charge-exchange event may be expected to consist of a fairly heavy proton prong of medium range and a very short He^3 prong. The four events under discussion show this feature. When a π^+ is absorbed by helium, on the other hand, one should usually see at least 2 energetic charged particles. The statistical argument given below in connection with the prong distribution from π^- interactions also indicates these π^+ interactions to be charge exchange. The possibility of radiative absorption by a single neutron is not yet excluded by these arguments but will be excluded shortly. With this identification of events the charge-exchange cross section for 53-Mev positive pions on helium is $\sigma_\gamma = 29 + 15$ millibarns. This cross section has been singled out because it is based on fairly direct evidence. Since the numbers of π^+ and π^- events at 53 and 68 Mev, respectively, are quite similar, taking into account the respective total observed paths through helium (see Tables II and III), we shall lump these data together for further discussion,

TABLE IV. Frequency of different types of interactions observed in helium.

Pion energy (Mev)	Electric charge	Elastic cases	Inelastic cases	Charge transfer: Charge exchange cases	Charge transfer: Absorption cases
53	pos.	6	2	4	1
68	neg.	4	2	5	
105	neg.	25	18	29	

referring to the average energy of 60 Mev. All cross sections thus calculated are listed in Table V, columns 1–4.

Although for π^- collisions with helium there is no way to distinguish between charge exchange and absorption for a single event without a magnetic field, a statistical argument favors an interpretation of σ_c mainly in terms of charge exchange. A meson can be absorbed by two or more nucleons[39,40] where some of the absorbing nucleons may remain bound together. In the center-of-mass system (cms) the statistical prong distribution is expected to be symmetric with respect to the backward and forward directions. The motion of the cms in the laboratory system distorts this distribution towards the forward direction. The degree of distortion has been calculated, for different angular distributions in the cms, with the result that at both energies considered here the ratio of the number of forward prongs to the number of backward prongs should be at most 1.5:1. Therefore one should observe not many more prongs in the forward direction than in the backward direction. Actually, at 60 Mev 9 prongs go forward and none backward, while at 105 Mev 23 prongs go forward and 6 backward, which is quite different from any distribution expected for non-radiative absorption. Similar calculations for the effect of radiative absorption by a single nucleon show that here a predominantly forward distribution might be expected. However, from results on photoproduction of mesons one can estimate for the inverse reaction a cross section of only about 0.5 mb. We therefore conclude that the observed charge-transfer events cannot be explained by radiative absorption by a single nucleon, few of them are due to absorption by two or more nucleons, and most are due to charge exchange. If, on the other hand, most of the charge-transfer events were to be ascribed to absorption by two or more nucleons some explanation of the observed forward prong distribution would have to be found.

TABLE V. Cross sections found experimentally for helium.

Pion energy (Mev)	1 σ_t(mb)	2 σ_e(mb)	3 σ_i(mb)	4 σ_s(mb)	5 σ_α(mb)	6 σ_γ(mb)
60 (av.)	89±18	37±12	15±8	37±12	15	22
105	207±24	74±14	51±12	82±12	20	62

Since helium in the ground state contains two protons with opposite spins and two neutrons with opposite spins, all charge-exchange events must be inelastic according to the Pauli principle. One would therefore expect that their prong distribution would look similar to the distribution of prongs for inelastic events. This is indeed shown by the diagram in Fig. 8, plotted for the 105-Mev data. Of the 18 inelastic events 8 show a single heavy prong going forward, while 10 show 2 heavy prongs. All 28 prongs are plotted. Of these 19 pass forward and 9 backward, compared with 23 forward and 6 backward for the charge-transfer events. Since the binding energy of the He^3 observed in the 8 single-prong inelastic events is the same as that of H^3 produced by charge exchange, one might expect that $29\times 8/18 = 13$ of the latter correspond to the 8 single-forward-prong inelastic events, leaving 16 events corresponding to the 10 double-prong inelastic events. The latter 10 events contain 9 heavy prongs going backward and 11 going forward. Thus for the remaining 16 charge-exchange events about 14 corresponding particles should pass backward and 18 forward. Due to exchange of charge only one-half of each of these groups can be visible as prongs in the cloud chamber. Therefore, from the prong distribution for inelastic events we infer that $13+9=22$ of the charge-transfer events should have forward prongs and 7 backward ones, in

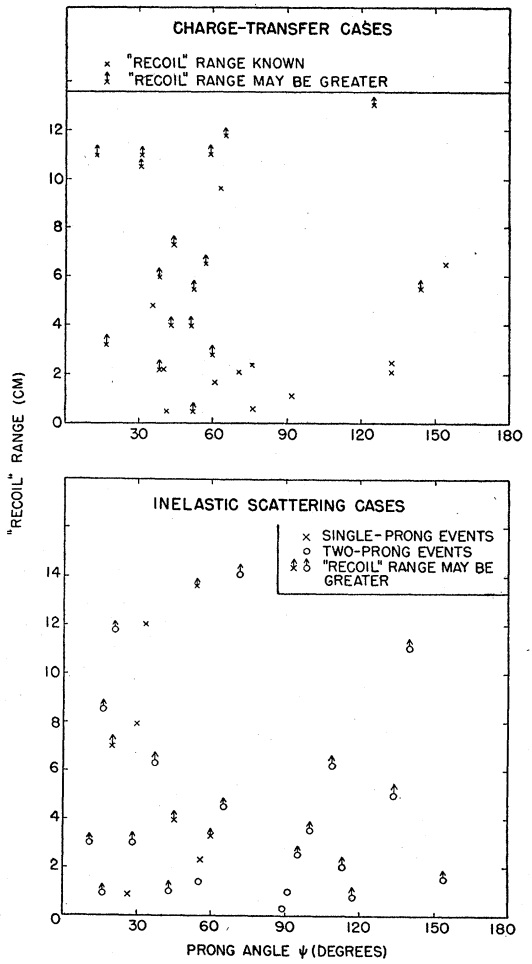

FIG. 8. Scatter diagrams of "recoil" ranges of heavy prongs for charge transfer and inelastic scattering, plotted from 105-Mev π^- helium results. Prong angle ψ is measured with respect to direction of incident pion track.

[39] F. L. Adelman, Phys. Rev. **85**, 249 (1952).
[40] S. Ruddlesden and A. Clark, Nature **164**, 487 (1949).

agreement with the observed distribution. Of course, because of the relatively small number of events studied here this agreement is partially fortuitous, and we cannot rule out that a fair portion of the events in question is caused by absorption. Another argument involving the magnitude of σ_e also favors the interpretation of the observed charge-transfer events given above and will be presented in Sec. VI C. Weighting all of the evidence presented we have arrived at the estimates for σ_γ and σ_α given in Table V, columns 5 and 6.

The apparently large charge-exchange cross section found here is not in agreement with results obtained by other authors for deuterium[41] and for heavier nuclei, from beryllium on up.[29,42,43] None of these authors report charge-exchange cross sections greater than a few millibarns.

The angular distribution of the elastically scattered mesons is given in Table VI. This table shows the data listed in two ways as functions of the cms-angles θ_0. For the ranges $0<\theta_0<60°$, $60°<\theta_0<120°$, and $120°<\theta_0<180°$ average differential cross sections $\Delta\sigma_e/\Delta\omega$ ($\Delta\omega=\omega_2-\omega_1=2\pi(\cos\theta_{01}-\cos\theta_{02})$) are given, while for the ranges $0<\theta_0<90°$ and $90°<\theta_0<180°$ "total" forward and backward cross sections are noted. Despite the large statistical errors, there appear to be two possibly significant features. At 60 Mev the scattering is almost completely backward, and at 105 Mev the scattering appears to be almost isotropic.

In the following sections an attempt will be made to interpret the present results in some more detail and to correlate them to the observed pion-nucleon cross sections.

B. General Considerations Concerning the Pion-Helium System

For the pion energies of 60 and 105 Mev the wavelengths in the cms of helium nucleus and pion are $\lambda\!\!\!^{-}_0=1.45\times10^{-13}$ and 1.04×10^{-13} cm, respectively. A radius for the nucleus can be defined by $R_1=A^{\frac{1}{3}}(\hbar/\mu_0 c)$, where A is the number of nucleons in the nucleus. For helium $R_1=2.21\times10^{-13}$ cm. Thus $\lambda\!\!\!^{-}_0$ and R_1 are almost equal, which implies that for the present case not much meaning can be attributed to a geometrical interpretation of R_1.

It follows quite generally from collision theory that

$$\sigma_e=A_n|1-C|^2, \tag{5}$$

and

$$\sigma_r=A_n(1-|C|^2), \tag{6}$$

where the "nuclear area" A_n is equal to πR_1^2 only if $\lambda\!\!\!^{-}_0\ll R_1$, and where C is a complex number with absolute value $\leqq 1$. C is related to the nuclear potential and is therefore of interest. One can write

$$C=|C|e^{2i\alpha}, \tag{7}$$

where α can be called the average phase shift of the scattered wave due to the nuclear potential. Therefore we have

$$\sigma_e=A_n(1-2|C|\cos2\alpha+|C|^2). \tag{8}$$

Although σ_e and σ_r have been measured, $|C|$ and α cannot be determined if A_n is not known. But since we have the condition that $|\cos2\alpha|\leqq1$ a lower limit for A_n can be found. From the data in Table V we obtain $A_n\geqq54\pm17$ mb at 60 Mev and $A_n\geqq147\pm29$ mb at 105 Mev. (πR_1^2 is equal to 154 mb.) Except for these lower limits for the nuclear area nothing can be said about C without further assumptions for A_n. Assuming different values for the nuclear radius R so that πR^2 is greater than the lower limits just determined for A_n we can make use of the "optical model"[44,45] in order to obtain estimated values for λ, the mean free path in nuclear matter, and V, the average potential between the helium nucleus and the pion. (Since $R\approx\lambda\!\!\!^{-}_0$ the "optical model" is not strictly valid here.) λ depends on $|C|$ only and V on α alone. Table VII shows the results. In this table λ was found from the graph $\sigma_r/\pi R^2$ *vs* KR in reference 44, with $\lambda=K^{-1}$, and V from the graph $\sigma_e/\pi R^2$ *vs* $\sigma_r/\pi R^2$ in reference 45, remembering that the quantity k_1 in reference 45 is determined by $V=1.97\times10^{-11}\beta k_1(1+\frac{1}{2}k_1\lambda\!\!\!^{-}_0)$ (where β is the pion velocity in the cms divided by c).

It is apparent that, while λ is quite sensitive to the assumed value of R, V is not. However, both quantities are much affected by the experimental uncertainties. Our values for V appear to agree with the values of 18 Mev reported for 62-Mev mesons[29] and 15 Mev reported for 48-Mev mesons[46] both found for carbon.

A considerable number of data would have to be available to allow more definite conclusions. By assuming that only s-wave and p-wave scattering is involved ($\lambda\!\!\!^{-}_0<R_1\lesssim2\lambda\!\!\!^{-}_0$), a conclusion can be drawn on the relative signs of the phase shifts of these waves at 60 Mev. (At 105 Mev the elastic scattering distribution appears to be compatible with a pure s-wave interaction.) Taking into account only s-waves and p-waves

TABLE VI. Elastic scattering angular distribution in helium.

Pion energy (Mev)	$\frac{\Delta\sigma_e}{\Delta\omega}\Big\|_0^{60°}$ (mb/sterad)	$\frac{\Delta\sigma_e}{\Delta\omega}\Big\|_{60°}^{120°}$ (mb/sterad)	$\frac{\Delta\sigma_e}{\Delta\omega}\Big\|_{120°}^{180°}$ (mb/sterad)	$\sigma_e\Big\|_0^{90°}$ (mb/sterad)	$\sigma_e\Big\|_{90°}^{180°}$ (mb/sterad)
60	1±1	0.6±0.6	10±4	7±5	30±11
105	7±3	6±2	4±2	40±10	34±10

[41] Roberts, Spry, and Tinlot, Bull. Am. Phys. Soc. **28**, No. 1, 14 (1953).
[42] R. Wilson and J. P. Perry, Phys. Rev. **84**, 163 (1951).
[43] Kessler, Byfield, Lederman, and Rogers, Bull. Am. Phys. Soc. **28**, No. 1, 14 (1953).
[44] Fernbach, Serber, and Taylor, Phys. Rev. **75**, 1352 (1949).
[45] H. A. Bethe and R. R. Wilson, Phys. Rev. **83**, 690 (1951).
[46] A. M. Shapiro, Phys. Rev. **84**, 1063 (1951).

TABLE VII. Mean free paths in nuclear matter and pion-helium potentials from "optical model."

Pion energy (Mev)	R (10^{-13} cm)	λ (10^{-13} cm)	V (Mev)
60	$=R_1=2.2$	7 ± 2	22 ± 11
	$=2\chi_0=2.9$	14 ± 4	17 ± 9
105	$=R_1=2.2$	$1.6^{+0.8}_{-0.3}$	17 ± 17
	$=3\chi_0=3.1$	6 ± 0.8	19 ± 10

the differential scattering distribution is

$$d\sigma_e/d\omega=\tfrac{1}{4}\chi_0^2[|b_0|^2+3(b_0b_1^*+b_0^*b_1)\cos\theta_0 +9|b_1|^2\cos^2\theta_0]. \quad (9)$$

Here $b_L=1-e^{2i\alpha_L-\delta_L}$, where α_L represents the phase shift corresponding to angular momentum number L (=0 or 1) and δ_L represents attenuation factors due to reactions that may take place. b_L^* is complex conjugate to b_L. The sign of the numerical value of the term multiplied by $\cos\theta_0$ determines whether forward or backward scattering predominates. In the present case this term is negative because of the observed strong backward scattering. One can show easily that therefore α_0 and α_1 must have opposite signs, indicating that repulsive as well as attractive potentials are involved in the scattering process.

Applying the isotopic spin formalism, one can give the pion isotopic spin $t=1$ with charge component $t_{13}=+1$ (for a negative meson taken as an example), and give the helium nucleus isotopic spin $T_1{}^N=0$ with $T_{13}{}^N=0$. Therefore the total charge is $T_3=T_{13}{}^N+t_{13}=+1$ and the total isotopic spin of the system is $T=t+T_1{}^N=1$. T and T_3 must remain constant throughout the collision process. After an elastic collision $T_2{}^N=T_1{}^N=0$ and $T_{23}{}^N=T_{13}{}^N=0$. After an inelastic collision resulting in up to 4 separate nucleons in addition to the pion, $T_2{}^N$ could be 0, 1, or 2. For $T_2{}^N=1$ one can have $T_{23}{}^N=1$, $t_{23}=0(T_3=T_{23}{}^N+t_{23}=+1)$ or $T_{23}{}^N=0$, $t_{23}=1$, the former reaction representing inelastic events with charge exchange ($t_{13}=1$, $t_{23}=0$), the latter concerning inelastic events without charge exchange. For each of these two possibilities one obtains[47] a probability of $\frac{1}{2}$. If one assumes that after a disruption of the helium nucleus the state $T_2{}^N=1$ prevails, the prediction is that $\sigma_\gamma=\sigma_i$. This is indeed indicated in Table V. For $T_2{}^N=2$ one can have $T_{23}{}^N=2$, $t_{23}=-1$, or $T_{23}{}^N=1$, $t_{23}=0$, or $T_{23}{}^N=0$, $t_{23}=1$. The first possibility would represent a double charge exchange turning a negative pion into a positive pion, the second possibility represents single charge exchange and the third simply inelastic events. The relative probabilities are 6:3:1, respectively. Since probably most of the interaction process is a result of individual collisions with the nucleons in the nucleus it appears that double charge exchange is quite unlikely even if one disregards any selection rules for $|T_2{}^N-T_1{}^N|$, and spin and parity considerations. Therefore probably $T_2{}^N=0$ or 1, in agreement with the experiment.

[47] E. U. Condon and G. H. Shortley, *Theory of Atomic Spectra* (Cambridge University Press, Cambridge, 1951), p. 76.

C. Helium Reactions in Terms of Pion-Nucleon Interactions

The ratio of the total cross section σ_t at 105 Mev to that at 60 Mev is 2.3 as inspection of Table V shows. Within the errors the same is true for the corresponding ratios of the partial cross sections σ_e, σ_i, and σ_c. Similar increases have been found for hydrogen as shown in Fig. 5 and for deuterium,[48] while for carbon and heavier nuclei the energy dependence is less marked.[9,49] One can conclude that the observed energy dependence of the cross sections for the light nuclei reflects the energy dependence of the π-nucleon cross sections as long as the interaction mean free path does not become small compared to the size of the nuclei. An attempt can therefore be made to explain the results for helium in terms of the observations on hydrogen.[9–14] Since the nucleons are bound, selection rules must apply limiting certain transitions, and the probability of a reaction of a given type must be determined in part by the number of final states accessible. In what follows such rules are not everywhere taken into account. However, mention will be made where a calculated result appears likely to be modified by a more complete treatment. $\pi^\pm$ proton nuclear forces are assumed to be identical in magnitude to $\pi^\mp$ neutron forces.

When a pion strikes a nucleon in a nucleus, the collision may be inelastic in the pion-nucleus system if the energy transfer from pion to nucleon is large. Thus for large scattering angles the differential elastic scattering cross section for the nucleus can become considerably smaller than the corresponding cross section for a single nucleon. This has been investigated theoretically by several authors.[50,51] The large-angle events that have been lost from the elastic scattering cross section contribute to the inelastic cross section. This partial cross section will be called σ_ρ. The other contribution to inelastic scattering is the result of pion-nucleon scattering with spin-flip, called here σ_φ so that $\sigma_i=\sigma_\rho+\sigma_\varphi$. In the p-state ($L=1$) the total angular momentum J of the pion-nucleon system is $J=L\pm S=1\pm\frac{1}{2}$, ($S=\frac{1}{2}$=nucleon spin). L, J, and the component of J, $m_j=m_L+m_S$, must remain constant. The possibility ($\Delta m_L=\pm1$, $\Delta m_S=\mp1$) results in a flip of the spin of the struck nucleon. Because of the Pauli principle an event of this kind taking place in helium must be inelastic just as for the case of charge exchange, as mentioned before. We finally can put $\sigma_r=\sigma_\alpha+\sigma_\gamma+\sigma_\rho+\sigma_\varphi$. All of the partial cross sections refer to the nucleus

[48] Anderson, Fermi, Nagle, and Yodh, Phys. Rev. **86**, 413 (1952).
[49] R. L. Martin, Phys. Rev. **87**, 1052 (1952).
[50] D. C. Peaslee, Phys. Rev. **87**, 862 (1952).
[51] M. Kawaguchi and Y. Yamaguchi (private communication).

as a whole. If σ_n stands for σ_α, σ_γ, σ_ρ, or σ_φ, we can call σ_n' the corresponding average cross section for an individual nucleon bound in the nucleus, where σ_n' represents σ_α', σ_γ', σ_ρ', or σ_φ'. Thus the σ_n' are defined as the cross sections for nucleons under the conditions prevailing in the particular nucleus under discussion. If there are equal numbers of neutrons and protons in the nucleus, and if we put σ_{nN}' and σ_{nP}' for neutrons and protons, respectively, then $\sigma_n'=\frac{1}{2}(\sigma_{nN}'+\sigma_{nP}')$. The quantity σ_α', particularly, is defined as one-half the average absorption cross section per nucleon pair in the nucleus. Since the range of the nuclear forces is limited and since the different types of interactions are in competition, we have $\sigma_r<(\sigma_\alpha'+\sigma_\gamma'+\sigma_\rho'+\sigma_\varphi')A$. However, one can write

$$\sigma_\alpha:\sigma_\gamma:\sigma_\rho:\sigma_\varphi=\sigma_\alpha':\sigma_\gamma':\sigma_\rho':\sigma_\varphi', \tag{10}$$

since the individual nucleon cross sections are proportional to the probabilities of occurrence for the different events and since these relative probabilities should not be changed by the fact that in the nucleus the different processes are in competition. It follows that

$$\sigma_n'=\sigma_n f, \tag{11}$$

where f is a constant for a given nucleus at a given pion energy. If some model, such as the "optical model" is assumed for the nucleus, with a given radius R, f can be calculated. As has been discussed, no such specific assumption can be made here since $\lambda_0\approx R$, and we will instead calculate f later from the experimental results. If all of the σ_n' are quite small, $f\approx 1/A$, of course. In the following paragraphs values for σ_γ' and σ_φ' will be calculated from information concerning pion-nucleon scattering, and a reasonable assumption can be made for σ_α', while more uncertainty exists about a calculation of σ_ρ'. From the equations [following from Eqs. (10) and (11)]

$$\sigma_\alpha'+\sigma_\gamma'=\sigma_c f, \tag{12}$$

and

$$\sigma_\rho'+\sigma_\varphi'=\sigma_i f, \tag{13}$$

we can, however, infer σ_ρ' in addition to f, making use of the calculated values of σ_γ', σ_φ', and σ_α', and the experimental values of σ_c and σ_i. (If σ_ρ' could be calculated with some certainty, Eqs. (12) and (13) could be used for a check of consistency.)

We shall proceed to calculate σ_γ'. Since charge exchange can take place only on either the neutrons or the protons in the nucleus, depending on the sign of the pion, the average cross section σ_γ' is one-half the pion-nucleon cross section for charge exchange. The nucleons in the nucleus can be assumed to move with an average kinetic energy $E_1=20$ Mev and a Gaussian momentum distribution[52] proportional to $\exp(-P^2/z)\,dp$, where P is the momentum, z is determined by E_1, and dp is a volume element in phase space. The charge-exchange cross section is given as a function of the relative energy between pion and nucleon by the graph, Fig. 5. Multiplication of the latter by the momentum distribution and numerical integration gives the upper limits for σ_γ' given in Table VIII, column 1. It may be of interest that the values thus calculated for pion energies of 60 and 105 Mev are 20 percent and 35 percent higher, respectively, than the values obtained if there were no nucleon motion.

One can argue that a pion-nucleon collision will result in a disruption of the helium nucleus with high probability if the pion loses more than 21 Mev in the process. (He^3 or H^3 have binding energies of 7 Mev leaving 21 Mev of the 28-Mev total binding energy of He^4 to be supplied.) Thus, only if the pion is scattered by a nucleon through a fairly large angle, is an inelastic collision possible relative to the pion-helium system. Considering the angular distribution for charge-exchange scattering[14] an integration through angles resulting in energy transfers greater than 21 Mev yields what might be considered more appropriate values for σ_γ'. These values are also given in Table VIII, column 1, below the upper limits given before.

TABLE VIII. Calculated values of partial pion-nucleon cross sections. For every number an upper limit is given as well as a value believed to be more appropriate, as discussed in the text.

	1	2	3	4	5	6
Pion energy (Mev)	σ_γ'(mb)	σ_φ'(mb)	σ_α'(mb)	f	σ_ρ'(mb)	σ_α(mb)
60	<9.0	<2.7	<8	<0.46±0.16	4.2±3.8	17±6
	6.0	0.8	>5	>0.30±0.10	3.7±3.5	17±6
105	<15.2	<13.2	<10	<0.31±0.07	$2.8^{+4.0}_{-2.8}$	32±8
	11.0	9.0	>7	>0.22±0.05	3.2±3.2	32±8

The spin-flip scattering cross section σ_φ' has been obtained by a similar calculation except that this type of scattering is not given explicitly but must first be inferred by means of a phase shift calculation. We shall use here the results of the phase shift analysis by Anderson *et al.*[14] Accordingly we have for the upper limit of σ_φ' at a particular energy

$$\sigma_\varphi'=\tfrac{3}{2}\pi\lambda_0^2[|A_\beta|^2+|A_{P\beta}|^2], \tag{14}$$

having integrated over the spin-flip angular distribution which is proportional to $\sin^2\theta_0$. λ_0 is here the wavelength in the pion-nucleon cms. A_β is the spin-flip scattering amplitude for a π^+ scattered by a proton, given by $A_\beta=\frac{1}{3}\sqrt{2}(e_{33}-e_{31})$ (in the notation used in reference 14), while $A_{P\beta}$ is the amplitude for a π^+ scattered by a neutron (or a π^- scattered by a proton), given by $A_{P\beta}=\frac{1}{9}\sqrt{2}(e_{33}-e_{31}+2e_{13}-2e_{11})$. The first index ($n$) on the contributing amplitudes e_{nm} is twice the total isotopic spin, and the second index (m) is twice the total angular momentum of the pion-nucleon system. e_{nm} is given by $1-e^{2i\alpha nm}$. The α_{nm} were obtained mostly by interpola-

[52] E. M. Henley, Phys. Rev. 85, 204 (1952).

tion between results given by Anderson *et al.*,[14] and partially from what few data are available at lower energies.[9–13,18] Integration over all nucleon momenta gives the upper limits for σ_φ' shown in Table VIII, column 2. The other values given here for σ_φ', considered to be more appropriate, were obtained by integration over large θ_0 only, corresponding to large energy transfers, as before for σ_γ'.

The cross section for absorption of a pion by a deuteron is about 8 mb at 60 Mev and about 10 mb at 105 Mev, as an interpolation of results on this reaction shows.[53,54] Byfield *et al.*,[29] have shown that these cross sections must be multiplied by a factor $\lesssim 3.3$ to obtain the cross section per proton in carbon. For helium we shall assume that this factor is between 1.5 and 2 because of the small number of nucleons present. The values for σ_α' (upper and lower limits per nucleon in helium) have been entered in Table VIII, column 3. From the values in Tables V and VIII and Eqs. (12) and (13) the values for σ_ρ' and f given in Table VIII, columns 4 and 5 have been calculated. The indicated errors are determined from the experimental uncertainty of σ_e and σ_i. From f and σ_α' one can calculate σ_α given in Table VIII, column 6. It is seen that these values for σ_α agree more or less with those already estimated from other considerations and given in Table V.

The value of f at 60 Mev should be smaller than that at 105 Mev since the individual nucleon cross sections are smaller at 60 Mev, and $f \to 1/A = 0.25$ for small nucleon cross sections. Taking into account the uncertainties in the assumptions made for the calculations and the large experimental uncertainties, the given values for f are not inconsistent with each other.

At both energies the values for σ_ρ' turn out to be rather small. σ_ρ' should increase with energy because at larger pion energies the energy transfer from a scattered pion to a nucleon becomes comparable to the binding energy of the nucleus for smaller scattering angles, in addition to the general increase of almost all of the pertinent cross sections with energy. Whether σ_ρ' indeed increases with energy cannot be recognized because of the large errors.

A more elaborate calculation applying the Pauli principle to the number of possible final states of the nucleons after an inelastic collision[55] and applying selection rules attributable to spin, isotopic spin, and parity considerations may reduce the computed values of σ_γ' and σ_φ' further. Since f must be >0.25, σ_γ' cannot be reduced very much at 105 Mev, while a greater modification might be possible at 60 Mev. If σ_γ' were almost zero at 105 Mev, σ_α' would have to be $>0.25 \times 82 = 20$ mb instead of the estimated value of 10 mb. This is an additional indication that a large portion of the observed "charge-transfer" events are caused by charge exchange.

[53] Clark, Roberts, and Wilson, Phys. Rev. **83**, 649 (1951).
[54] Durbin, Loar, and Steinberger, Phys. Rev. **83**, 646 (1951).
[55] M. H. Johnson, Phys. Rev. **83**, 510 (1951).

D. Pion-Helium Elastic Scattering in Terms of Pion-Nucleon Scattering

Both the protons and the neutrons in the nucleus contribute to the elastic scattering of pions. The amplitudes due to these two contributions interfere so that the total differential scattering distribution is given by

$$d\sigma_e/d\omega = \tfrac{1}{4}\lambda_0^2[|B_t|^2 + 3(B_t A^*_{\alpha t} + B_t^* A_{\alpha t}) \times \cos\theta_0 + 9|A_{\alpha t}|^2 \cos^2\theta_0]\Omega, \quad (15)$$

where $B_t = B + B_P$ for the s-waves and $A_{\alpha t} = A_\alpha + A_{P\alpha}$ for the p-waves. Furthermore,

$$B = e_3,\ e_3 = 1 - e^{2i\alpha_3},$$
$$B_P = \tfrac{1}{3}(e_3 + 2e_1),\ e_1 = 1 - e^{2i\alpha_1},$$
$$A_\alpha = \tfrac{1}{3}(2e_{33} + e_{31}),$$
$$A_{P\alpha} = \tfrac{1}{9}(2e_{33} + e_{31} + 4e_{13} + 2e_{11}).$$

Here it is important to note that the signs of the individual phase shifts as determined from pion-proton scattering may or may not have to be reversed for pion-neutron scattering. For instance, the nuclear force between a π^- and a proton may be attractive while the force between a π^+ and a neutron may be equal in magnitude but repulsive. Some meson theories lead to such results.[45] Calculations have been carried out for both possibilities.

The factor Ω in Eq. (15) takes into account the presence of several proton-neutron pairs, the term in brackets applying only to one such pair, as well as the possible reduction of the cross section for large energy transfers[50,51] (large θ_0). No attempt is made to calculate exactly the magnitude and dependence on θ_0 of Ω.

The phase shifts α_{nm} must be selected for the proper energies. A pion of given laboratory energy has considerably more energy with respect to a bound nucleon in the pion-helium cms than it has in a free-nucleon-pion cms. Assuming merely that an elastic collision consists of a pion striking a single nucleon bound rigidly in the helium nucleus, the present pion-helium results at 60 and 105 Mev may have to be compared with the pion-proton results at energies as high as 78 and 137 Mev, respectively. Values for the corresponding pion-proton phase shifts[14] are given in Table IX. Pion-neutron phase shifts are assumed to be equal in magnitude, but possibly with opposite signs, as mentioned above. Putting $\Omega = 1$ the scattering due to a neutron-proton pair (σ_e') in the helium nucleus can be calculated. Table X gives the results. The assumption of neutron phase shifts with signs opposite to those given in Table IX seems to represent well the apparently strong backward scattering observed at 60 Mev.

To calculate the final elastic cross sections the values in Table X must be modified. For Ω we are assuming an empirical value of 1.6 which will result in agreement between calculated and experimentally observed values

TABLE IX. Phase shifts used for calculation of elastic pion-helium scattering.

Pion energy (Mev)	Corresponding free-proton-pion energy (Mev)	α_3	α_1	α_{33}	α_{31}	α_{13}	α_{11}
60	78	−6°	+9°	+15°	+3°	0	0
105	137	−15°	+11°	+40°	+6°	+2°	−5°

for σ_e at 60 Mev. The effect of large energy transfers on the angular distribution is still neglected.

An important modification must be made to take into account the diffraction scattering caused by the inelastic reactions discussed in the previous section. This effect will here be taken into account only approximately. We first express $B_t\Omega^{\frac{1}{2}}$ and $A_{\alpha t}\Omega^{\frac{1}{2}}$ in Eq. (15) by terms equal to $(1-e^{2i\beta_0})$ and $D(1-e^{2i\beta_1})$, respectively. The quantities β_0, β_1, and D must be determined so that $d\sigma_e/d\omega$ is properly reproduced. Next, we substitute for $B_t\Omega^{\frac{1}{2}}$ and $A_{\alpha t}\Omega^{\frac{1}{2}}$ the expressions $(1-e^{2i\beta_0-\delta_0})$ and $D(1-e^{2i\beta_1-\delta_1'})$, respectively. The reaction cross section is given by

$$\sigma_r=\pi\lambda\!\!\!^{-}_0{}^2[(1-e^{-2\delta_0})+3D^2(1-e^{-2\delta_1'})]. \qquad (16)$$

The term $D^2(1-e^{-2\delta_1'})$ can be expressed more simply by a term $(1-e^{-2\delta_1})$. The average attenuation factors δ_0 and δ_1 are related to each other by the relative "distances" traveled by the pion through the nucleus in the s- and p-states, respectively. (For diffraction scattering we again assume that only s- and p-wave scattering occurs. This seems justified since $\lambda\!\!\!^{-}_0<R_1\lesssim 2\lambda\!\!\!^{-}_0$. For the same reason, however, no definite geometry, as is used here, applies in a strict sense.) From the geometry of a sphere of radius $R_1=2.2\times10^{-13}$ cm one infers that here for averages $\delta_1\approx\frac{1}{2}\delta_0$. Equation (16) can now be solved for δ_0, putting σ_r equal to its observed values. For the different quantities defined we have $\beta_0=-12.4°$ and $-24.5°$, $\beta_1=25.6°$ and $30°$, $D=0.43$ and 1.27, $\delta_0=0.16$ and 1.2, and $\delta_1'=0.19$ and 0.43, for 60 and 105 Mev, respectively. The latter calculations were carried out for n-phase shifts opposite to p-phase shifts only, since Table X shows that only for this case one can expect to obtain large backward/forward ratios. One finds the values in Table XI for the elastic scattering cross section of helium with diffraction scattering taken into account in this way.

Comparison with the data in Tables V and VI shows that at 60 Mev the calculated and experimental values for $\sigma_e|_0^{90°}$ and $\sigma_e|_{90°}^{180°}$ are not inconsistent. The calculated value for σ_e at 105 Mev is 100 percent too large while the backward/forward ratio is about 50 percent too small. Comparison of Tables X and XI shows that the interference with the diffraction scattering makes the scattering intensities considerably more pronounced in the forward direction. This makes it difficult to understand large backward/forward scattering ratios if the latter should be verified by further experiments on helium. Particularly, assumptions for Ω to take into account the reduction of $d\sigma_e/d\omega$ at large θ_0, due to large energy transfers, would further reduce the expected backward scattering. However, σ_ρ', the inelastic cross section due to large energy transfers which must be related to Ω, is fairly small as shown in Table VIII. This may mean that Ω would not have to decrease very much for large θ_0.

So far interference with Coulomb scattering has been neglected. The importance of this effect for the smaller angles ($<50°$) has been shown for pion-proton scattering[56] and for pion-carbon scattering.[29,50] By adding the approximate Coulomb-scattering amplitude $\pm 2i/[137\beta\sin^2(\frac{1}{2}\theta_0)]$ to the s- and p-wave scattering amplitudes considered in the previous paragraphs, one can estimate that for helium Coulomb scattering is important below $\theta_0'=35°$ at 60 Mev, and below $\theta_0'=25°$ at 105 Mev. Below θ_0' the differential scattering distributions may be increased or decreased considerably, depending on the sign of the scattered pions and on the direction of the nuclear forces. However, the solid angle between our lower limit of observation ($\theta_0=20°$) and θ_0' is so small that few events are expected in this interval. Similar considerations apply to scattering in hydrogen. Thus, for the present work, neglecting Coulomb effects seems justified.

VII. CONCLUSIONS

Assuming that all types of interactions between pions and the helium nucleus are due to interactions between pions and the individual nucleons in the nucleus, an approximate calculation based mostly on the phase shifts found from experimental results on pion-proton scattering shows that a fairly consistent picture can be constructed, resulting generally in rough agreement between calculated and observed cross sections. The estimated experimental absorption cross section agrees with that estimated from the pion-deuteron absorption cross section, leaving most of the observed charge-transfer events to be interpreted as due to charge

TABLE X. Calculated elastic scattering cross sections for a neutron-proton pair.

Pion energy (Mev)	Charge	σ_e' (mb)	$\sigma_e'\|_0^{90°}$ (mb)	$\sigma_e'\|_{90°}^{180°}$ (mb)
60	n-phase shifts same as p-phase shifts	58	27	31
	n-phase shifts opposite to p-phase shifts	24	4	20
105	n-phase shifts same as p-phase shifts	170	81	89
	n-phase shifts opposite to p-phase shifts	120	40	80

[56] L. Van Hove, Phys. Rev. 88, 1358 (1952).

exchange. Some of the inelastic scattering observed can be accounted for by pion-nucleon scattering with spin flip. The relatively large backward-to-forward elastic scattering ratio shows that not much inelastic scattering can be due to pion-nucleon collisions with energy transfers large enough to disrupt the nucleus. The relatively small elastic scattering cross sections, together with the high backward-to-forward scattering ratios, indicate that protons and neutrons in the nucleus scatter with opposite phase shifts. Throughout the computations only s-wave and p-wave scattering has been considered. Particularly at 105 Mev some scattering corresponding to higher angular momenta ($L=2, 3$) may take place. Also many effects due to the bound state of the nucleons have been neglected. A modification affecting all aspects of pion-helium scattering may be introduced by a consideration of multiple scattering inside the helium nucleus as recently worked out for a two-body system by Brueckner.[57]

The authors wish to acknowledge several inspiring conversations on some of the subjects covered in this article with R. Serber and D. C. Peaslee. We are very grateful to E. T. Booth and J. Rainwater for the opportunity to work at the Nevis cyclotron. The untiring cooperation of the cyclotron operating staff under J. Spiro is greatly appreciated. Furthermore, we are indebted to W. F. Goodell, L. M. Lederman, and A. Pevsner for giving us most valuable advice on details of operation with the cyclotron. We also wish to express our thanks to the members of the Brookhaven National Laboratory, without whose support this work would not have been possible. In particular, the diffusion chamber was constructed mostly in the cloud chamber shop under S. G. Hasselriis. W. A. Tuttle and F. W. Rothery were responsible for most of the construction and operation of the electric control circuits. K. J. Kristoffersen contributed much toward the operation of the diffusion chamber and the management of the expeditions to the cyclotron. M. R. Burns and F. S. Keene scanned most of the pictures.

[57] K. A. Brueckner, Phys. Rev. **89**, 834 (1953).

TABLE XI. Calculated elastic scattering cross sections for helium.

Pion energy (Mev)	σ_e (mb)	$\sigma_e\|_0^{90°}$ (mb)	$\sigma_e\|_{90°}^{180°}$ (mb)
60	37	13	24
105	140	100	40

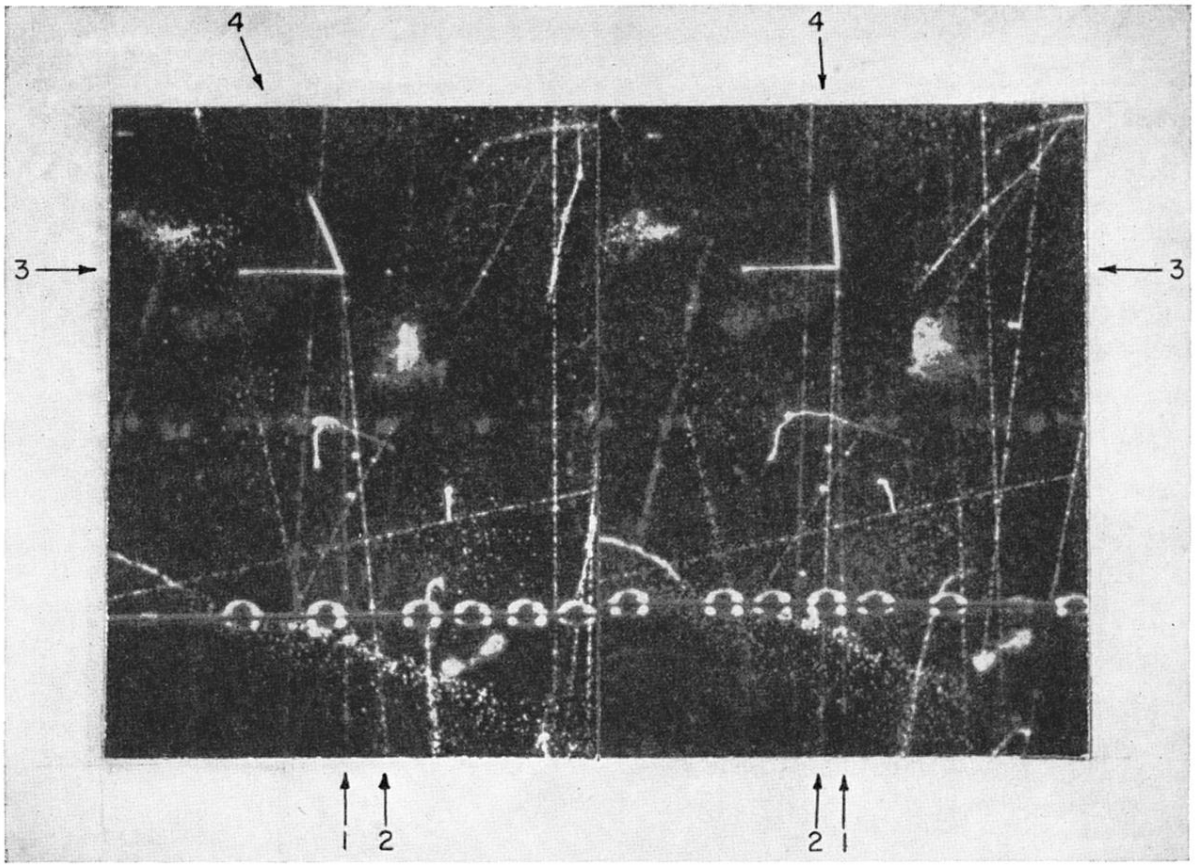

FIG. 6. Photograph of a 105-Mev negative pion scattered inelastically in helium. Tracks 1 and 2 show incident and scattered pions, respectively. Tracks 3 and 4 are two charged recoils, both stopping in the gas.

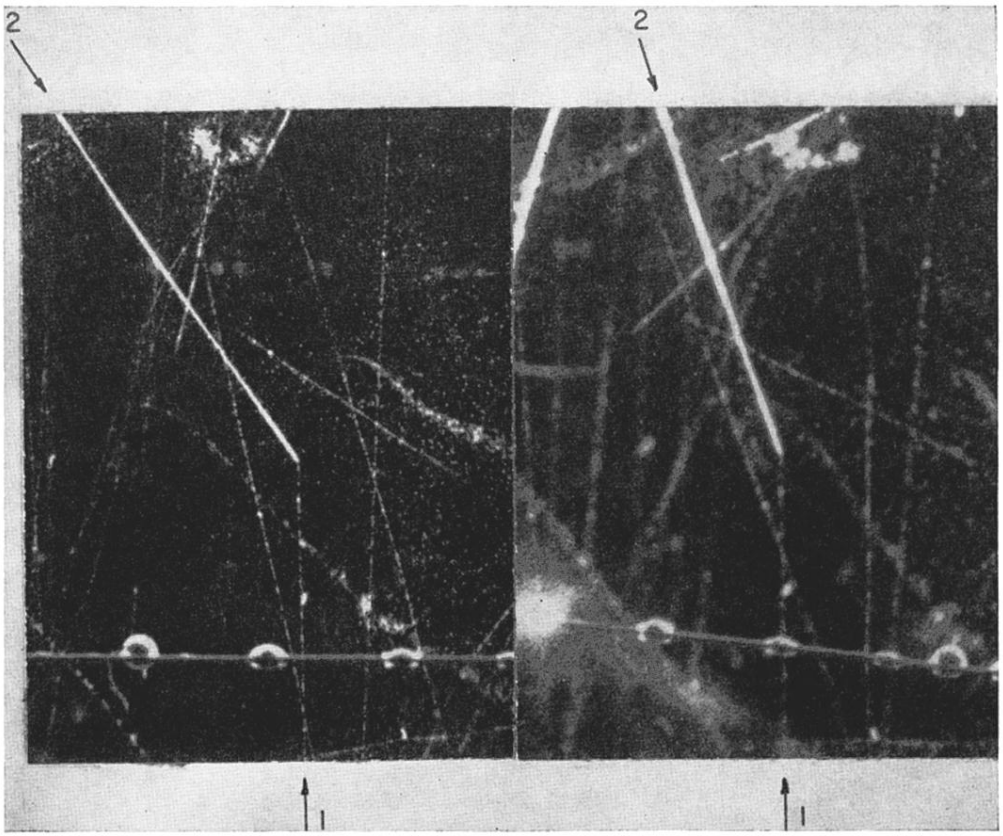

FIG. 7. Photograph of charge exchange or absorption of a 105-Mev negative pion. Track 1 is the incident pion and Track 2 is the only charged recoil.